



# Cold Spring Harbor Protocols

## All-Optical In Situ Histology of Brain Tissue with Femtosecond Laser Pulses

Philbert S. Tsai, Pablo Blinder, Jeffrey A. Squier and David Kleinfeld

*Cold Spring Harb Protoc*; doi: 10.1101/pdb.prot073858

---

### Email Alerting Service

Receive free email alerts when new articles cite this article - [click here](#).

---

### Subject Categories

Browse articles on similar topics from *Cold Spring Harbor Protocols*.

[Cell Imaging](#) (444 articles)  
[Fluorescent Proteins](#) (216 articles)  
[Imaging for Neuroscience](#) (233 articles)  
[Immunofluorescence](#) (32 articles)  
[Mouse](#) (256 articles)  
[Multi-Photon Microscopy](#) (72 articles)

---

---

To subscribe to *Cold Spring Harbor Protocols* go to:  
<http://cshprotocols.cshlp.org/subscriptions>

---

## Protocol

# All-Optical In Situ Histology of Brain Tissue with Femtosecond Laser Pulses

Philbert S. Tsai, Pablo Blinder, Jeffrey A. Squier, and David Kleinfeld

This protocol describes the application of laser pulses to image and ablate neuronal tissue for the purpose of automated histology. The histology is accomplished in situ using serial two-photon imaging of labeled tissue and removal of the imaged tissue with amplified, femtosecond pulses. Together with the use of endogenous fluorescent indicators and/or deep penetration of antibody labels and organic dyes, this method may be used to automatically image, reconstruct, and vectorize structures of interest across millimeter to centimeter regions of brain with micrometer resolution.

## MATERIALS

---

It is essential that you consult the appropriate Material Safety Data Sheets and your institution's Environmental Health and Safety Office for proper handling of equipment and hazardous materials used in this protocol.

**RECIPES:** Please see the end of this article for recipes indicated by <R>. Additional recipes can be found online at <http://cshprotocols.cshlp.org/site/recipes>.

## Reagents

Blocking solution for brain tissue <R>  
Cyanoacrylate cement (Superbonder 49550; Loctite)  
4',6-diamidino-2-phenylindole (DAPI) dilactate (Sigma-Aldrich D9564)  
Fluorescent antibodies  
Fluorescent gel solution <R>  
Mice (see Discussion for examples of strains that have been used)  
Paraformaldehyde (PFA), 4% (w/v), in PBS  
Phosphate-buffered saline (PBS; Sigma-Aldrich)  
Saline (0.9% NaCl)

## Equipment

Charge-coupled device (CCD) camera (Pantera 1M60, Dalsa Corp.)  
Coverslips  
Diode array capable of emitting 630-nm light

---

Adapted from *Imaging in Neuroscience* (ed. Helmchen and Konnerth). CSHL Press, Cold Spring Harbor, NY, USA, 2011.

© 2013 Cold Spring Harbor Laboratory Press

Cite this article as *Cold Spring Harb Protoc*; 2013; doi:10.1101/pdb.prot073858

Imaging setup with the following components (see Fig. 1A for integration of the imaging and ablation optomechanical setup):

- Imaging laser source

*One of two commercially available Ti:sapphire laser oscillators are used. The Mira-F900, pumped by a Verdi V-10 (Coherent Inc.) delivers 10-nJ 100-fsec pulses at a repetition rate of 78 MHz. Alternatively, the Tsunami HP, pumped by a 15-W Millennia (Spectra-Physics) delivers 25-nJ 100-fsec pulses at a repetition rate of 80 MHz. Each system has a separate pump and oscillators, instead of all-in-one systems, so that the pump beam focus in the Ti:sapphire rod may be realigned to compensate for potential deterioration in laser power over many months of operation.*

- Ablation laser source

*A commercially available Ti:sapphire amplified laser system is used. The Libra is an all-in-one system that includes a Vitesse seed oscillator and a regenerative Ti:sapphire amplifier pumped with an Evolution Q-switched Nd:YLF laser (Coherent Inc.). This system delivers 200- $\mu$ J 100-fsec pulses at a repetition rate of 5 kHz. A potential alternative ablation source is the RegA 9000 amplifier system (Coherent Inc.). This system provides a 200-kHz train of pulses with a few microjoules of energy, which is sufficient for plasma-mediated ablation, although it is slightly less energy than we use for our current experimental configurations.*

- Two-photon laser scanning microscope

*A custom-built microscope is used based on a design derived from the original in vivo system, which was constructed by Denk (Svoboda et al. 1997). The custom design (Tsai and Kleinfeld 2009) allows integration of the imaging and ablation beams through a polarizing beam splitter (Fig. 1B). The microscope is operated by a custom-designed control software suite, MPscope (Nguyen et al. 2006, 2009), that incorporates a scripting language for automation of the multiple steps in the all-optical histology sequence (Fig. 1C). Imaging is performed using a dipping objective with a high numerical aperture (NA; 0.5–1.0).*

- Fast programmable translation stages

*The tissue is mounted on a set of fast translation stages, capable of speeds up to 8 mm/sec with micrometer accuracy (XYR-4040, Danaher Motion). The stages are interfaced to the computer system through a set of Galil DMC-4040 controllers (Galil Motion Control Inc.) that raster the tissue across the focus of the objective lens. Centimeter-sized tissue volumes may be ablated, and multiple fields of view may be imaged using two-photon laser-scanning microscopy (TPLSM) (Fig. 1A).*

Perfusion equipment (see Step 4)

Piezoelectric device

Razor blade mounted to a precision translation stage

## METHOD

*We focus on the region of cortex that codes the sensory input from the rodent vibrissae, but the procedures are applicable for all brain areas.*

### Mapping the Region of Interest

*Localize and identify barrels in the mouse somatosensory cortex with maps of the intrinsic optical signal in response to single-vibrissa stimulation (Frostig et al. 1993).*

1. Stimulate a single vibrissa with a piezoelectric device while the skull is illuminated with 630-nm light from a diode array (Drew and Feldman 2009).
2. Capture the backscattered light on a CCD camera.

*The response is defined as the optical signal averaged over the 0.5–1.5-sec epoch after stimulation, whereas baseline is defined as the signal averaged over the 1.0-sec epoch that starts 1.0 sec before the onset of stimulation.*

3. Divide the response signal by the baseline signal at each pixel to generate a map of the functional representation of the stimulated whisker. The response is registered relative to the surface vasculature.

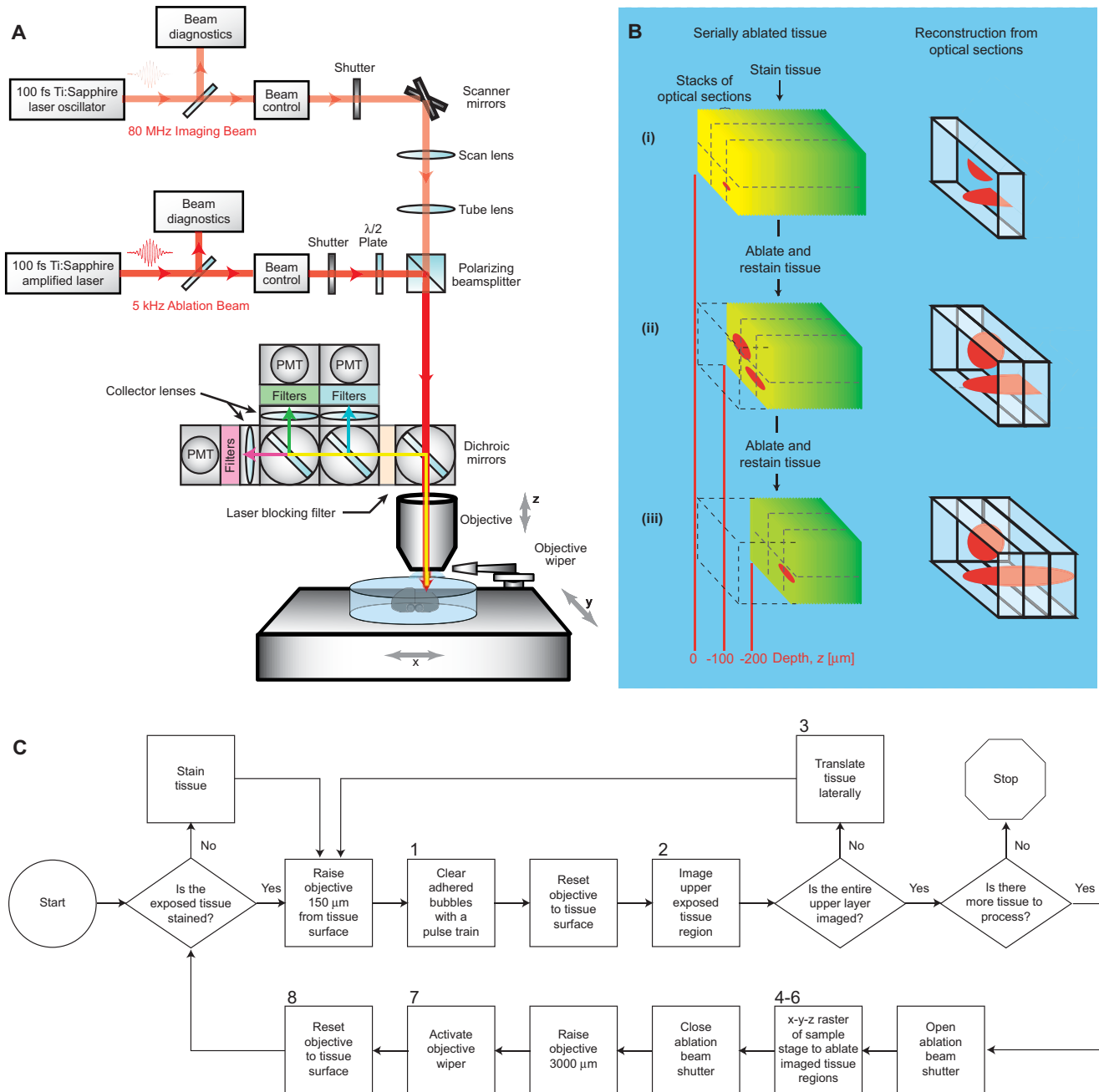


**FIGURE 1.** Overview of all-optical histology. (A) Schematic of laser and imaging systems. An 80-MHz train of 100-fsec pulses from an optically pumped Ti:sapphire oscillator are directed with scanning mirrors to image a preparation placed on a programmable translation stage. A 5-kHz train of amplified 100-fsec pulses is coupled into the microscope with a polarizing beam splitter and directed to the sample for ablation. Beam control of both beams includes intensity and beam profile modifications. The tissue is moved laterally by the programmable translation stages to allow ablation over large areas as well as imaging over multiple fields of view. (B) Schematic illustration of the iterative process of all-optical histology. (i) The tissue sample (*left* column) containing two fluorescently labeled structures is imaged by conventional two-photon laser scanning microscopy to collect optical sections. Sections are collected until scattering of the incident light reduces the signal-to-noise ratio below a useful value; typically this occurs at  $\sim 150 \mu\text{m}$  in fixed tissue. Labeled features in the resulting stack of optical sections are digitally reconstructed (*right* column). (ii) The top of the now-imaged region of tissue is completely ablated with amplified femtosecond laser pulses to expose a new surface for imaging. The sample is again imaged down to a maximal depth, and the new optical sections are added to the previously stored stack. (iii) The process of ablation and imaging is again repeated so that the structures of interest can be fully sectioned and reconstructed. (C) Flowchart of the all-optical histology process. (*Legend continues on following page.*)

## Perfusing with Fluorescent Gel

4. Perfuse rodent transcardially at 0.3 mL/sec with 50 mL of saline (0.9% NaCl) at 37°C.
5. Switch perfusion to 50 mL of 4% (w/v) PFA in PBS, followed again by 50 mL of saline.
6. Perfuse the animal with a fluorescent gel solution.
7. Extract the brain and postfix it for 20 h in 4% (w/v) PFA in PBS at 4°C.

*Fixation of the fluorescently labeled tissue keeps the label from leaking after slabs of tissue are prepared (in Step 8).*

## Blocking and Staining

8. Guided by the results from the intrinsic optical signal to define the region of interest, cut an ~1.5-mm-thick coronal slab of tissue from the extracted brain using a razor blade mounted to a precision translation stage.
9. Incubate the slab of tissue for 10–12 h in blocking solution.
10. Incubate in 1 µg/mL of DAPI dilactate and the specific antibodies of choice that are directly conjugated to a fluorophore (Tsai et al. 2009b).

*For example, we have stained with anti-NeuN conjugated to Alexa-594 (custom order, Chemicon); the incubation lasted for 4 d at room temperature with the goal of complete staining throughout the thick slabs. Finally slabs were washed in PBS.*

## Subblocking and Mounting

11. Subblock the thick coronal slab over the region of interest.
12. Mount the block to a coverslip using a thin layer of cyanoacrylate cement.
13. Once the cement has cured, immerse the entire sample in PBS and transfer it to the all-optical histology rig.
14. Image the sample using a dipping objective having a high NA (i.e., 0.5–1.0) (Fig. 1A).

*In our work this is centered on the vibrissa barrel field.*

## Iterative Imaging and Ablation

15. The iterative process of imaging and ablation is laid out as a flowchart in Figure 1C, and technical details pertaining to particular steps are provided in the legend. Examples of cutting parameters that have been used for sample ablation with 1 and 5 kHz trains of 100-fsec pulses are provided in

**FIGURE 1.** (Continued) The following notes apply: (1) Hydrolysis bubbles formed by the ablation process can adhere to the tissue surface, and diminish subsequent imaging quality. The application of a single burst of 500 amplified laser pulses targeted to the solution above the tissue surface acts to clear the bubbles from the tissue surface. (2) Laser power should be increased approximately exponentially with depth to compensate for scattering and absorption losses. (3) The translation stages are programmed to move to an adjoining lateral field of view for imaging. It is useful to allow roughly 10%–20% spatial overlap with previously imaged fields of view to verify proper registration. (4) The translation stages are programmed to perform a raster scan across the entire lateral extent of the tissue. Parameters for ablation can be varied to trade off between speed and precision. Higher pulse energies can allow faster translation speed and larger step sizes, but may increase the surface roughness of the tissue, thereby potentially reducing the quality of subsequent images. (5) To maximize spatial overlap, so as to minimize surface roughness, the lines of ablation in successive planes can be interlaced by offsetting the start position in each plane by one-half of the lateral step size between lines. (6) The depth of tissue to be removed per ablation round will depend on the tissue scattering properties and the strength of the fluorescent signal. It is important to ablate less depth than was imaged in the previous imaging round, as a means to verify registration. (7) Hydrolysis bubbles resulting from the ablation process can drift upward and adhere to the front surface of the objective. These bubbles are removed by raising the objective and sweeping a lens-tissue wiper across the objective with an automated servo motor. (8) On occasion, the dipping of a dry objective into immersion solution can result in the trapping of a large air bubble under the objective surface. This can be ameliorated by dipping the objective twice without a wipe step between dips.

**TABLE 1.** Ablation parameters that have been used with 100-fsec pulses

Objective NA	Pulse repetition rate (kHz)	Energy ( $\mu$ J)	Translation speed ( $\mu$ m/sec)	Lateral step size ( $\mu$ m)	Axial step size ( $\mu$ m)	Volume rate ( $\text{mm}^3/\text{sec}$ )
0.8 Dipping	5	4	4.0	10	10	$4 \times 10^{-4}$
0.5 Dipping	1	2	4.0	2.5	10	$1 \times 10^{-4}$
0.5 Dipping	1	8	4.0	10	10	$4 \times 10^{-4}$
0.3 Dipping	1	22	4.0	10	50	$20 \times 10^{-4}$
0.2 Air	1	33	1.5	10	20	$3 \times 10^{-4}$

Table 1. Note that these parameters represent cutting speeds that are overly conservative by a factor ranging from 2 to 10.

## DISCUSSION

We describe the coupling of plasma-mediated ablation, driven by laser pulses of  $\sim 100$  fsec, with two-photon microscopy for the purpose of performing serial histology of neuronal tissue (Tsai et al. 2003). This combined procedure, together with related labeling and analysis techniques, extends the histological use of two-photon microscopy to image tissue throughout arbitrarily thick samples.

The ablation of tissue with femtosecond infrared laser pulses requires large optical fluences, in excess of  $1 \text{ J}/\text{cm}^2$  (Tsai et al. 2009a). Such high fluences can be achieved with commercially available  $\sim 100$ -MHz laser oscillators with  $\sim 100$ -fsec pulse duration and a pulse energy of  $\sim 10$  nJ when the beam is focused with high NA objectives to a  $1\text{-}\mu\text{m}$  diameter spot. Such beams have been used for fine-scale ablation of subcellular structures (Tirlapur and Konig 2002; Yanik et al. 2004). For large-scale ablation, practical issues suggest the use of microjoule-scale pulse energies. These are obtained by amplifying individual nanojoule seed pulses with an optical amplifier to form pulses with femtosecond duration, but with energies of  $1\text{--}100 \mu\text{J}$ , albeit at repetition rates of only  $1\text{--}100$  kHz. Amplified pulses have been used to ablate a wide variety of tissues, including cornea (Loesel et al. 1996; Oraevsky et al. 1996; Juhasz et al. 1999; Lubatschowski et al. 2000; Maatz et al. 2000), dental tissue (Loesel et al. 1996; Neev et al. 1996), skin (Frederickson et al. 1993), and brain (Loesel et al. 1996, 1998; Suhm et al. 1996; Goetz et al. 1999; Tsai et al. 2003). The focus in our laboratory is on data acquisition from brain tissue that has been structurally labeled. Examples in this article are taken from results in our laboratory.

### Laser Alignment

One technical issue concerns the centering and alignment of the imaging and ablation beams. The collimation and alignment of the ablation beam is adjusted by telescopes and routing mirrors located within the amplified beam path. The microscope objective is temporarily replaced by a  $45^\circ$  mirror that deflects both imaging and ablation beams to a target at least 30 cm away. We align the ablation beam to the imaging beam at both the distant target and the back focal plane of the objective. This ensures colocalization of the foci of the two beams at the center of the imaging field. Alignment can be verified by ablating and imaging the top of a glass slide immersed in a fluorescent dye.

### Example Applications

We have used all-optical histology to visualize the three-dimensional structure of the cortical vasculature in mice and the location and identity of surrounding cells. Figure 2A shows the raw overlay of four iterations of imaging and ablation on cortical tissue from a transgenic mouse expressing cyan fluorescent protein in endothelial cells. The technique has been extended to tissue volumes in excess of a cubic millimeter, as shown in Figure 2B for a C57Bl6 mouse with gel-perfused vasculature. Here,



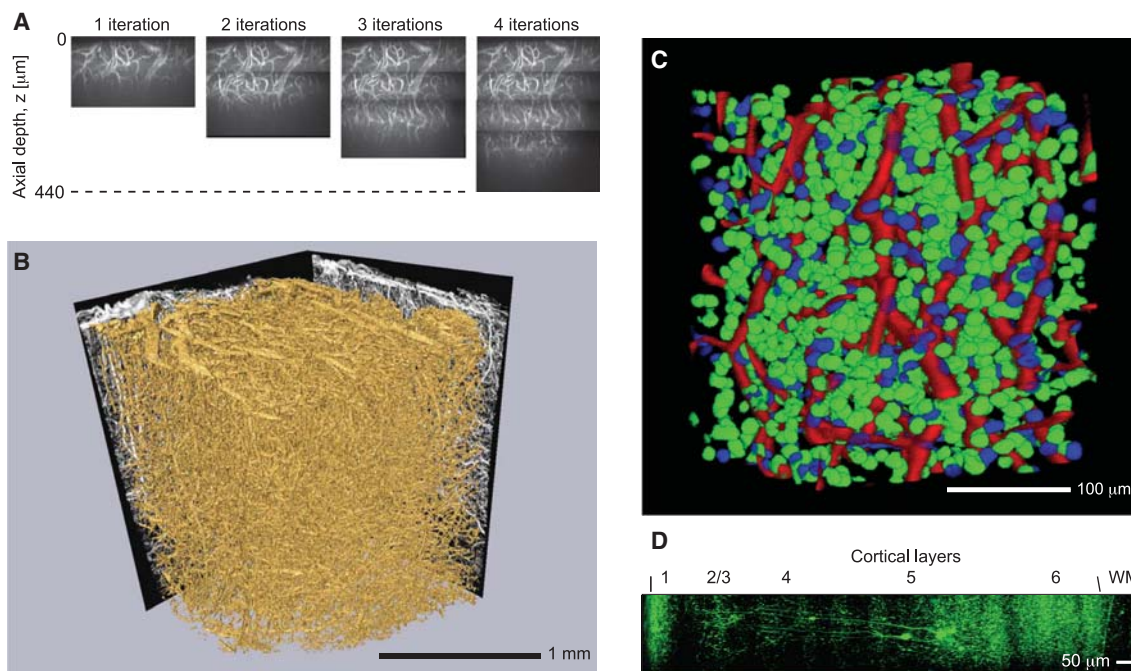


**FIGURE 2.** Examples of the application of all-optical histology. (A) Serial reconstruction of vasculature in a block of neocortex of a transgenic mouse in which actin filaments in the vascular wall are endogenously labeled with cyan fluorescent protein. Four successive cutting and imaging cycles are shown. The laser was focused onto the cut face with an intermediate numerical aperture (0.5 NA) objective and a raster pattern was used to optically ablate successive planes at a depth of 10  $\mu\text{m}$  each with total thicknesses of 70  $\mu\text{m}$  per cut. The energy per pulse varied from 0.4 to 1.7  $\mu\text{J}$ . Each stack of images represents a maximal side projection of all accumulated optical sections. The sharp breaks in the images shown in successive panels demarcate the cut boundaries. (Adapted from Tsai et al. 2003). (B) Large volume (1.5  $\text{mm}^3$ ) reconstruction of block-face data obtained from mouse neocortex. The vasculature was filled with fluorescein-labeled gel. Ablation was performed with pulse energies of 5  $\mu\text{J}$  and rastering of the translation stage, as in A. The image data consisted of overlapping stacks,  $256 \times 256 \times 120 \mu\text{m}$ , that were registered into a single volume by means of cross-correlation over nearest neighbor features in the overlap region. (C) A  $200 \times 200 \times 150\text{-}\mu\text{m}$  volume extracted from a larger reconstruction of mouse cortical vasculature and surrounding cell nuclei. Volume-accurate vascular reconstructions are shown in red, neuronal nuclei are shown in green, and non-neuronal nuclei are shown in blue. (D) Iterative processing of a block of neocortex of a transgenic mouse with neurons labeled by yellow fluorescent protein. Twenty-four successive cutting and imaging cycles are shown. The laser was focused onto the cut face with a  $20\times$  magnification 0.5 NA dipping objective, and a raster pattern was performed at 4 mm/sec to optically ablate successive planes at a depth of 10  $\mu\text{m}$  each with total thicknesses between 40 and 70  $\mu\text{m}$  per cut. The energy per pulse was maintained at 8  $\mu\text{J}$ . Each stack of images represents a maximal side projection of all accumulated optical sections obtained using TPLSM at  $\lambda = 920 \text{ nm}$ . Anatomical layers are labeled above the figure, including the cortical layers (1–6) and the white matter (WM).

each individual imaging field was  $256 \times 256 \mu\text{m}$  wide, extended 120  $\mu\text{m}$  into the tissue, and overlapped with neighboring fields by 56  $\mu\text{m}$  laterally and 80  $\mu\text{m}$  axially. A  $5 \times 5 \times 25$  array of imaging fields was merged to reproduce the full tissue volume. Additionally, we simultaneously localized all of the cell nuclei using DAPI and identified neurons and non-neuronal cells using an Alexa-conjugated antibody to the neuronal specific antigen NeuN (Fig. 2C).

To show the ability to visualize fine neuronal processes, we have applied all-optical histology to layer 5 pyramidal neurons from mouse neocortex obtained from the transgenic mouse strain B6.Cg-TgN(thy1-YFPH)2Jrs (Feng et al. 2000), available from The Jackson Laboratory. The result of 24 iterations of imaging and ablation along the radial axis of neocortex is shown in Figure 2D. The imaging in each iteration progressed in the dorsal to ventral direction (left to right in the figure), over a single  $200 \times 200 \mu\text{m}$  field of view through at least 100  $\mu\text{m}$  of tissue depth. The ablation also progressed from the dorsal to ventral direction, removing an average of 60  $\mu\text{m}$  per iteration. Each image stack was then projected along the coronal direction and overlaid to produce the composite image.

## Advantages and Limitations

The primary advantage of the all-optical histological technique is the ability to image large volumes of unfrozen and unembedded soft tissue in an automated, unsupervised fashion. The potential for tissue distortion and misalignment owing to the generation of thin physical sections is eliminated, allowing for straightforward image registration and generation of three-dimensional maps and reconstructions.

The technique is limited to fluorescently labeled tissues whose optical properties are amenable to two-photon microscopy; that is, the scattering depth must be large compared with the axial extent of the focal volume. The speed of TPLSM imaging is currently the time-limiting aspect of this technique (Tsai et al. 2003). At the imaging speeds used in our experiments, acquisition of 1 mm<sup>3</sup> of image data takes 30 min to 5 h, depending on the degree of imaging overlap desired for registration. By comparison, at the ablation speeds used in our experiments, removal of 1 mm<sup>3</sup> of tissue requires 40 min.

Both imaging and ablation times may be shortened in the future. To calculate the theoretical limit for the speed of imaging, we consider the imaging of cellular nuclei labeled with DAPI. At a 1:5 binding ratio of DAPI to DNA base pairs, and assuming that the 3 million base pairs in the mouse genome are uniformly distributed within a 100 μm<sup>3</sup> nuclear volume, each 1 μm<sup>3</sup> voxel would contain 6000 fluorophores. Operating at 20% of the dye saturation, and assuming a 10% collection efficiency for a 0.8 NA objective, and 1% total transmission and photoconversion efficiency for the microscope (Tsai and Kleinfeld 2009), each laser pulse would generate ~10 photoelectrons, and thus a single-voxel signal-to-noise ratio of ~3. It is therefore reasonable to consider the imaging limit of one laser pulse per voxel. For an 80-MHz laser system, this results in an imaging time of 3 h for a 0.5 cm<sup>3</sup> whole mouse brain at 1 μm<sup>3</sup> sampling. With regard to ablation, the current time could be substantially reduced by the use of structured illumination (Oron et al. 2005). Thus, if one considers only strong fluorophores so that ablation is the rate limiting step, the rate of all-optical histology comes to ~20 h per 0.5 cm<sup>3</sup> mouse brain.

## RECIPES

### *Blocking Solution for Brain Tissue*

10% (v/v) normal goat serum  
2% (v/v) Triton X-100  
0.1% (w/v) sodium azide  
Mix contents in phosphate-buffered saline (PBS).

### *Fluorescent Gel Solution*

Albumin-fluorescein isothiocyanate conjugate (Sigma-Aldrich)  
Phosphate-buffered saline (PBS; Sigma-Aldrich)  
Gelatin from porcine skin, type A (Sigma-Aldrich G1890)

1. Prepare a 2% (w/v) solution of gelatin by boiling in PBS followed by cooling to <50°C.
2. Combine with 1% (w/v) albumin-fluorescein isothiocyanate conjugate, maintained with stirring at 40°C.
3. Filter through filter paper (no. 1 Whatman) that has been pre-moistened with PBS.
4. Warm the filtered solution to 40°C before the perfusion.

## ACKNOWLEDGMENTS

We thank Beth Friedman for help with the deep antibody staining and John P. Kaufhold for his work on associated analysis of the histology data. This work was funded by the National Institutes of Health (grants EB003832, MH72570, and MH085499 to D.K.) and a ISF-Bikura postdoctoral fellowship to P.B.



## REFERENCES

- Drew PJ, Feldman DE. 2009. Intrinsic signal imaging of deprivation-induced contraction of whisker representations in rat somatosensory cortex. *Cereb Cortex* 19: 331–348.
- Feng G, Mellor RH, Bernstein M, Keller-Peck C, Nguyen QT, Wallace M, Nerbonne JM, Lichtman JW, Sanes JR. 2000. Imaging neuronal subsets in transgenic mice expressing multiple spectral variants of GFP. *Neuron* 28: 41–51.
- Frederickson KS, White WE, Wheeland RG, Slaughter DR. 1993. Precise ablation of skin with reduced collateral damage using the femtosecond-pulsed, terawatt titanium-sapphire laser. *Arch Dermatol* 129: 989–993.
- Frostig RD, Dory Y, Kwon MC, Masino SA. 1993. Characterization of functional organization within rat barrel cortex using intrinsic signal optical imaging through a thinned skull. *Proc Natl Acad Sci* 90: 9998–10002.
- Goetz MH, Fischer SK, Velten A, Bille A, Strum V. 1999. Computer-guided laser probe for ablation of brain tumours with ultrashort laser pulses. *Phys Med Biol* 44: N119–N127.
- Juhasz T, Loesel HL, Kurtz RM, Horvath C, Bille JF, Mourou G. 1999. Corneal refractive surgery with femtosecond lasers. *IEEE J Sel Top Quant Electron* 5: 902–910.
- Loesel FH, Niemez MH, Bille JF, Juhasz T. 1996. Laser-induced optical breakdown on hard and soft tissues and its dependence on the pulse duration: Experiment and model. *IEEE J Quant Electron* 32: 1717–1722.
- Loesel FH, Fischer JP, Gotz MH, Horvath C, Juhasz T, Noack F, Suhm N, Bille JF. 1998. Non-thermal ablation of neural tissue with femtosecond laser pulses. *Appl Phys B* 66: 121–128.
- Lubatschowski H, Maatz G, Heisterkamp A, Hetzel U, Drommer W, Welling H, Ertmer W. 2000. Application of ultrashort laser pulses for intrastromal refractive surgery. *Graefes Arch Clin Exp Ophthalmol* 238: 33–39.
- Maatz G, Heisterkamp A, Lubatschowski H, Barcikowski S, Fallnich C, Welling H, Ertmer W. 2000. Chemical and physical side effects at application of ultrashort laser pulses for intrastromal refractive surgery. *J Opt A* 2: 59–64.
- Neev J, Carrasco WA, Armstrong WB, Da Silva LB, Feit MD, Matthews DL, Perry MD, Rubenchik AM, Stuart BC. 1996. Applications of ultrashort pulse lasers for hard tissue surgery. *IEEE J Sel Top Quant Electron* 2: 790–800.
- Nguyen Q-T, Tsai PS, Kleinfeld D. 2006. MPScope: A versatile software suite for multiphoton microscopy. *J Neurosci Methods* 156: 351–359.
- Nguyen Q-T, Dolnick EM, Driscoll J, Kleinfeld D. 2009. MPScope 2.0: A computer system for two-photon laser scanning microscopy with concurrent plasma-mediated ablation and electrophysiology. In *Methods for in vivo optical imaging*, 2nd ed. (ed. RD Frostig), pp. 117–142. CRC Press, Boca Raton, FL.
- Oraevsky A, Da Silva L, Rubenchik A, Feit M, Glinesky M, Perry M, Mammini B, Small W, Stuart B. 1996. Plasma mediated ablation of biological tissues with nanosecond-to-femtosecond laser pulses: Relative role of linear and nonlinear absorption. *IEEE J Sel Top Quant Electron* 2: 801–809.
- Oron D, Tal E, Silberberg Y. 2005. Scanningless depth-resolved microscopy. *Opt Express* 13: 1468–1476.
- Suhm N, Gotz MH, Fischer JP, Loesel F, Schlegel W, Sturm V, Bille JF, Schroder R. 1996. Ablation of neural tissue by short-pulsed lasers—A technical report. *Acta Neurochir* 138: 346–349.
- Svoboda K, Denk W, Kleinfeld D, Tank DW. 1997. In vivo dendritic calcium dynamics in neocortical pyramidal neurons. *Nature* 385: 161–165.
- Tirlapur UK, Konig K. 2002. Targeted transfection by femtosecond laser light. *Nature* 418: 290–291.
- Tsai PS, Kleinfeld D. 2009. In vivo two-photon laser scanning microscopy with concurrent plasma-mediated ablation: Principles and hardware realization. In *Methods for in vivo optical imaging*, 2nd ed. (ed. Frostig RD), pp. 59–115. CRC Press, Boca Raton, FL.
- Tsai PS, Friedman B, Ifarraguerri AI, Thompson BD, Lev-Ram V, Schaffer CB, Xiong Q, Tsien RY, Squier JA, Kleinfeld D. 2003. All-optical histology using ultrashort laser pulses. *Neuron* 39: 27–41.
- Tsai PS, Blinder P, Migliori BJ, Neev J, Jin Y, Squier JA, Kleinfeld D. 2009a. Plasma-mediated ablation: An optical tool for submicrometer surgery on neuronal and vascular systems. *Curr Opin Biotechnol* 20: 90–99.
- Tsai PS, Kaufhold J, Blinder P, Friedman B, Drew P, Karten HJ, Lyden PD, Kleinfeld D. 2009b. Correlations of neuronal and microvascular densities in murine cortex revealed by direct counting and colocalization of nuclei and vessels. *J Neurosci* 29: 14553–14570.
- Yanik MF, Cinar H, Cinar HN, Chisholm AD, Jin Y, Ben-Yakar A. 2004. Functional regeneration after laser axotomy. *Nature* 432: 822.